Sensors & Actuators: B. Chemical 404 (2024) 135185

Contents lists available at ScienceDirect

Sensors and Actuators: B. Chemical

journal homepage: www.elsevier.com/locate/snb

Concentration gradients probed in microfluidics by gate-array electrolyte organic transistor

Gulseren Deniz Saygin [a,b], Pierpaolo Greco [a,c,*], Meenu Selvaraj [d], Michele Di Lauro [a], Mauro Murgia [a,e], Michele Bianchi [f], Luciano Fadiga [a,c], Fabio Biscarini [a,f]

[a] Center for Translational Neurophysiology - Istituto Italiano di Tecnologia, Via Fossato di Mortara 17–19, I-44100 Ferrara, Italy
[b] Department of Physics, Informatics and Mathematics, Università degli Studi di Modena e Reggio Emilia, Via Campi 103, I-41125 Modena, Italy
[c] Department of Neurosciences and Rehabilitation, Università di Ferrara, Via Borsari 46, I-44121 Ferrara, Italy
[d] MTA, Medical Trials Analysis Italy S.r.l., Via Ariosto 28, I-44121 Ferrara, Italy
[e] Istituto per lo Studio dei Materiali Nanostrutturati (ISMN-CNR), Via Gobetti 101, I-40129 Bologna, Italy
[f] Department of Life Sciences, Università degli Studi di Modena e Reggio Emilia, Via Campi 103, I-41125 Modena, Italy

ARTICLE INFO

Keywords:
Organic electronics
Microfluidics integration
Electrolyte-gated organic field effect transistor (EGOFET)
Self-assembled monolayer

ABSTRACT

We propose a device architecture termed gate-array electrolyte gated organic transistor (GA-EGOFET) that quantitatively measures the solute concentration gradient created in a spatially inhomogeneous solution, for instance a (biological) fluid. The integrated H-cell microfluidics yields a diffusive concentration profile along the microfluidics channel according to the flow rate of the input streams. We demonstrate this concept by monitoring the formation of self-assembly monolayers (SAMs) on top of an array of parallel Au gate electrodes exposed to a different local concentration of alkanethiols. The deposition rate and the coverage both increase from the entrance towards the H-cell end. The voltage change at each gate is transduced in the transfer curve acquired with the specific gate electrode. For short chain length SAMs (n = 3), the trend of the current hints to a diffusion-limited surface reaction. For longer thiols (n = 6, 9), instead, the slower surface diffusion or incorporation in the more stable and compact SAM yields a current that is independent of the longitudinal gradient. The microfluidics/GA-EGOFET platform is viable for constructing dose curves in reproducible manner and for validating different electrode functionalization strategies where the deposition rates are different at each substrate site.

1. Introduction

Microfluidics is the science and technology of systems that process or manipulate micro or nanolitre fluid volumes by flowing them into channels whose dimensions are from tens to hundreds of micrometres [1]. Microfluidics were used in various application areas like chemical and biological analysis, point of care devices, and drug development, even for the generation of biofunctional interfaces in molecular diagnostic devices [2–4]. Recent applications include lab-on-a-chip, organ (oid) on-a-chip, and analog logic processing.

1D silicon based nanowires transistor [5], as well as 2D graphene based FETs [6] have been extensively studied for small biomolecule detection, pH measurements, but few works have considered the effect of solution concentration gradients developing in the reaction volume. Also tunnel FETs high sensitivity, based on the steepness of the transfer in the subthreshold region, is greatly affected by the bio-analyte concentration control, because of the charge screening effects [7]. Microfluidic devices can be employed to generate controlled stable concentration gradients when the sensing chamber or electrode is placed in convective flow or even just under diffusion controlled transport [8], with mechanism based on multiple concurrent streams [9], or modification of the surface tension of the boundary walls of the fluidic device via electroactive thin molecular layer [10]. Besides performance, monitoring concentration gradients is important per se, for example in process involving plasma filtration, and has been achieved by probing the dielectric properties of the medium using differential transformers [11] or ion sensitive FETs [12].

Integration of microfluidics with transistor-based biosensors gathered lots of interest since they simplify the sample transport, reagent mixing or the immobilization of biorecognition molecules, or the

* Corresponding author at: Center for Translational Neurophysiology - Istituto Italiano di Tecnologia, Via Fossato di Mortara 17–19, I-44100 Ferrara, Italy.
E-mail address: pierpaolo.greco@unife.it (P. Greco).

https://doi.org/10.1016/j.snb.2023.135185
Received 25 September 2023; Received in revised form 15 December 2023; Accepted 17 December 2023
Available online 21 December 2023

subsequent delivery of the targeted biomarkers to the transducer interface [13–17]. Electrolyte gated organic field-effect transistors (EGOFET) are fabricated with organic semiconductor and they exploit the large capacitive coupling of the electrical double layers (EDLs) at the interfaces with the semiconductive channel and with the gate electrode [18–21]. The gate electrode potential is sensitive to antigen binding recognition molecules at the surface. For the biosensing with EGOFET, the functionalization of the gate electrode with the biorecognition groups for the target has become the most consolidated strategy for biorecognition [22,23]. Several functionalization strategies on the gate electrode were successfully demonstrated, like grafting of antibodies or aptamers either by the Protein G or by self-assembled monolayers (SAMs) [24,25]. Integration of EGOFET with microfluidic devices enables the detection of multiple biomarkers by miniaturization and multiplexing gate electrodes [26,27].

SAMs form a thin, tightly packed, robust interface on the surface of noble metals such as gold, and are widely studied in organic electronics [28,29]. Their use in organic electronics is not only for the gate functionalization, but also for the tailoring of charge injection at Source and Drain electrodes. A better alignment of SAMs and the organic semiconductor energy levels causes more efficient charge injection [30]. The gate functionalization with SAMs has also impact on the device characteristics, since dipole moments of SAMs shift the work function of the gate electrode, thus determining the flat band potential and the threshold voltage of the device. Investigating the formation of SAMs was quite important for improving the functionalization protocols and the device performance.

The formation of SAMs on the gold gate depends not only on the chemical structure of the molecules but also on how they come in contact with the transducer surface. Microfluidics help to deliver the thiol molecules to the transducer surfaces, so that the kinetics of the formation and the overall duration of incubation can be used to modulate the surface coverage [31].

The idea here is to devise a compact miniaturized experimental setup, by integrating an array of gate electrodes EGOFET (GA-EGOFET) with a H-cell microfluidics, that enables controlled growth, deposition, or delivery from a solution. Our setup allows us to control two relevant experimental parameters, viz. the deposition rate and the deposition time, and vary them systematically through the local concentration at different substrates. The number of samples N that are prepared and monitored within a ***single experiment*** is limited by the number of gate electrodes and the design of the microfluidics channel.

2. Materials and methods

2.1. Fabrication of the GA-EGOFET

The gate electrodes are fabricated starting from a thin flexible foil of Kapton metalized with gold (Creavac, Dresden, DE). The metalized polymeric foil has a thickness ranging between 50 and 100 μm. Either polymethylmethacrylate (PMMA) or polyimide (PI) were used as alternative substrate. The metallization layer is composed by a thin adhesive film of chromium (3 nm) and a sputtered gold film 70 nm thick. The metalized gold foil was then patterned by means of laser scan ablation to obtain an array of rectangular gate electrodes with dimensions 4 mm × 1 mm. After ablation, the flexible electrode array was sonicated in ethanol for 5 min in order to remove all the residues generated by the laser process. The test pattern contained interdigitated Source and Drain electrodes, with channel length L= 20 μm and width W= 67850 μm, so W/L= 3400. A film of organic semiconductor 6,13-Bis(triisopropylsilylethynyl)pentacene (TIPS-pentacene) was deposited on the channel by drop casting a 0.5 μl droplet of TIPS-pentacene solution (20% toluene, 80% hexane), that was left to dry.

2.2. Fabrication and integration of the microfluidic devices

The EGOFET is integrated with two microfluidic devices. The first is a closed pool, positioned on the transistor channel and made with a small eye-shaped chamber whose overall dimensions are 5 mm × 1 mm x 3 mm, obtained as a replica of a 3D master printed with 3D printer based on digital light processing, B9 Creator v1.2 (B9Creations, US). Polydimethylsiloxane (PDMS) was poured inside the master and then cured at room temperature for one day. After the curing, the PDMS chamber was peeled off. Two vias for inlet and outlet of liquid were punched on the PDMS chamber and were connected to external pump systems by means of PEEK tubing with internal diameter equal to 500 μm.

The second microfluidic device is an H-cell, designed with CAD and fabricated with the laser lithography. The geometry is designed according the COMSOL simulations of the H-cell. A thick vinyl based double side adhesive (TESA from Beiersdorf AG, Hamburg, Germany) was cut with an IR laser operated at 7 W power, pulse repetition frequency 30 Hz. After laser cutting, the excess of adhesive was removed to expose the fluidic microchannel. A top layer of PMMA was processed with laser lithography to prepare the top boundary of the fluidic cell.

2.3. Self-assembly monolayers (SAMs)

Thiolated molecules were purchased from Merck KGaA. Solutions of 3-Mercapto-1-propanol (MP), 6-Mercapto-1-hexanol (MH) and 9-Mercapto-1-nonanol (MN) were obtained solubilizing thiols in PBS buffer 1x solutions. Before any use, all thiols were diluted up to 1 μM concentration (pH= 7.2).

2.4. Electrical characterization and evaluation of the transfer curves

The electrical characterisation was performed by Source -Measurement Unit (SMU) Agilent B2912 (California, U.S.A) with two channels. The transfer curves were recorded in order, starting from gate 1 to gate 6. The gate electrodes were measured before and after flow of solution containing thiols. Transfer curves were obtained by measuring channel current (I_{ds}) upon sweeping Gate-Source voltage in the range from 0 V to −0.6 V with steps of −1 mV at a fixed Drain-Source voltage V_{ds}= −0.2 V.

2.5. Green channel image acquisition

The picture snapshots of the array of gate electrodes where acquired operating the microfluidic H-cell with the thiol stream solution including E102–131 dye in aqueous solution, with dilution ratio equal to 1 μl of dye solution in 10 ml of thiol-PBS solution. After injecting the two streams in the H-cell the flow was stopped and the images were acquired with a video microscope at the same time of EGOFET characterization, with the objective fixed on magnification of G5 and G6 of the array. The green channel of each image was analysed with ImageJ to extract the intensity averaged on the electrode area.

2.6. Electrochemistry setup

Cyclic Voltammetry measurements were performed in a 5 mM solution of $[Fe(CN)_6]3-/4-$ with a CH Instrument potentiostat model 760 c. A three-electrode cell contained the Au/Kapton gate as working electrode (WE), a Pt wire as a counter electrode (CE) and an Ag/AgCl electrode (Elbatech, Livorno Italy) as a reference electrode (RE). The CV measurements were performed in the voltage range between − 0.20 V and 0.45 V with the different scan rates (0.01 V/s, 0.05 V/s, 0.1 V/s, 0.15 V/s, 0.2 V/s). The gold electrodes tested have the geometric area of 4 mm^{-2} and were immersed and incubated in different vials with different SAMs for 10 min.

3. Results

3.1. Architecture of the EGOFET integrated with microfluidic H-cell

The H-cell was extensively used to study laminar flow and the formation of a diffusion gradient. The H-cell comprises a long channel with two inlets and two outlets. The schematic geometry of the microfluidic H-cell and the assembled microfluidic H-cell/GA-EGOFET device is shown in Fig. 1. The alignment of the substrate with the array of gate electrodes and the adhesive microfluidics yields an almost equal area of each gate electrode exposed to the solution inside the H-cell. The lower half of the main channel of the microfluidic H-cell, where solvent stream flows, runs across the top ends of the gate electrodes; the thiol solution flows along the upper half of the main channel instead.

In the typical EGOFET architecture, the gate is immersed in the electrolyte on top of the transistor channel at short distance from the semiconductor channel. In the present architecture, the gates are placed in the H-cell. The electrolyte contained in the PDMS pool placed on top of the organic semiconductor channel is connected to the inlet of the solvent in the H-cell. This electrolyte bridge connection is obtained with a flexible silicon tubing and is actuated by a syringe pump, pushing the PBS buffer from the PDMS pool to the H-cell inlet. To test the transistor current dependence on the length of the electrolyte tubing, segments of interconnecting tubes with different lengths were employed and transfer curves recorded. The I_{ds} current decreases after 30 cm and shows a saturated behaviour afterwards. (See Fig. S3 in Supporting Information).

3.2. Study of the concentration gradients

The fluids entering at the inlets move along the channel by laminar flow, as the Reynolds number $\mathrm{Re} = \frac{\rho u \ell}{\mu}$ ranges between 10^{-3} and 0.1, for the flow rates employed in the experiment, viz. 2, 10, 20 and 50 μl/min. Here ρ is the density, μ is the viscosity, u the mean velocity and ℓ is the height of the channel. Thus, the mixing inside the H-cell occurs by diffusion across the interface formed by the two parallel fluid streams, as there are neither active (e.g. piezoelectric valves, acoustic waves, moving elements or actuators like magnetic ciliae, rotors, etc [32–34] nor passive elements (pillars, fillers, meanders, microstructures [35–37] to cause sizable turbulence.

The two fluid streams flow along the same direction in laminar flow regime by the action of an external syringe pump. One of the fluid streams consists of a concentrated PBS solution containing a SAM forming molecule (red color stream at the bottom left in Fig. 2a-c), the other with the PBS electrolyte buffer (blue color stream at the bottom right in Fig. 2a-c). The SAM forming molecules diffuse across the interface between the two fluids until they are adsorbed at the gate electrode at the opposite side of the microfluidics where the solvent stream flows. At the flow rate used here, complete mixing along the channel does not occur. The H-cell microfluidics yields a smooth gradual diffusive interface along the microfluidics channel from the inlet to the outlet, with a concentration gradient across (and perpendicular to the) microfluidics channel. Indeed, the solute concentration decreases from the solute stream to the solvent stream, and a smooth longitudinal gradient of the SAM forming molecules is established, with their concentration decreasing in the solute stream while increasing in the solvent stream from the inlet to the outlet.

We solve the system of Navier Stokes and convection diffusion equations for the H-cell microfluidic device reported in Supporting Information by finite element modelling (FEM), where we input the values of the relevant parameters shown in Table 1.

Viscosity of the medium is detrimental for diffusion limited reactions, even if thermodynamic equilibrium constant is not affected [38]. In case of thiol solutions, the chain length per se is not modifying the viscosity in the range of concentration and temperature adopted for the study. Electron transfer reaction rate by electrodes covered with SAMs is generally reduced by the viscosity of the medium, in a way dependant on the alkyl chain length.[39] However we do not include this variable in the modelling, considering that the final application would be detection in sample extracted from physiological fluids, with μ comprised between 1 and 1.3 mPa·s approximately.

We assume that the diffusion coefficient will exhibit approximately the same value $D = 6 \times 10^{-10}$ $\mathrm{m^2/s}$ for all SAMs studied, since for homolog series with n = 3…9, we expect D to vary from + 40% for n = 3 to − 30% for n = 9 with respect to the value n = 6 [31] based on the inverse square root dependence on molecular mass:

$$D_m = D_n \sqrt{\frac{MW_n}{MW_m}} \tag{1}$$

Both stationary and time-dependent problems were solved and the output was recorded specifically for the coordinates (x_G, y_G) of the points representing the gates immersed in the channel, highlighted in Fig. 2i.

In the gate array the positions are labelled after gate position G1 and G2 (near inlets, center axis at y_G=1.5 and 3 mm respectively), G3 and G4 (in the middle of mixer channel, center axis at y_G=11 and 16 mm respectively), G5 and G6 (near outlets, center axis at y_G=24 and 29 mm respectively). For sake of simplifying the discussion, we disregard the finite size of the gate electrodes (that integrates across the concentration gradient across a finite area) and discuss the concentration profiles in space and time at the different values of y_G. The steady-state concentration c vs x and their gradient dc/dx for three different flow rates are shown in Fig. 2a-c. The fastest flow rate (Fig. 2a) yields the steepest

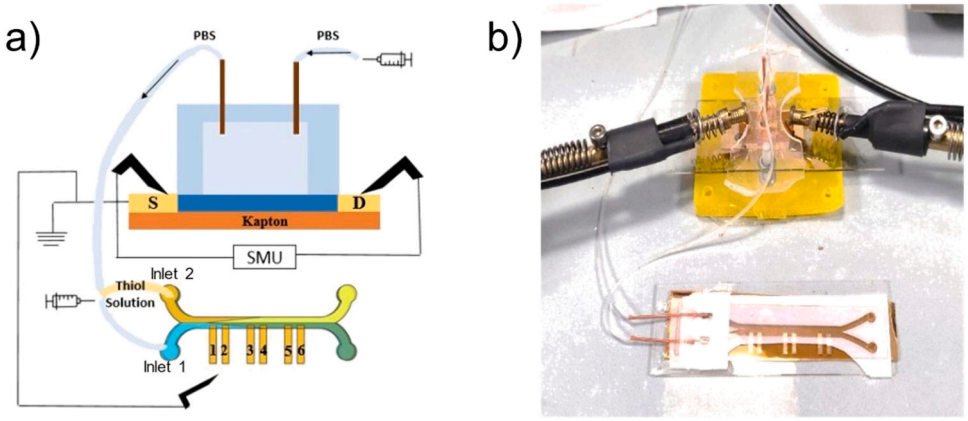

Fig. 1. a) Schematic drawing of the integration between EGOFET and H-cell, with the electrolyte bridge between the outlet of the microfluidic cell on top of the semiconductor and the solvent stream inlet of the H-cell, b) Picture of the GA-EGOFET with Source and Drain in contact with measurement probes.

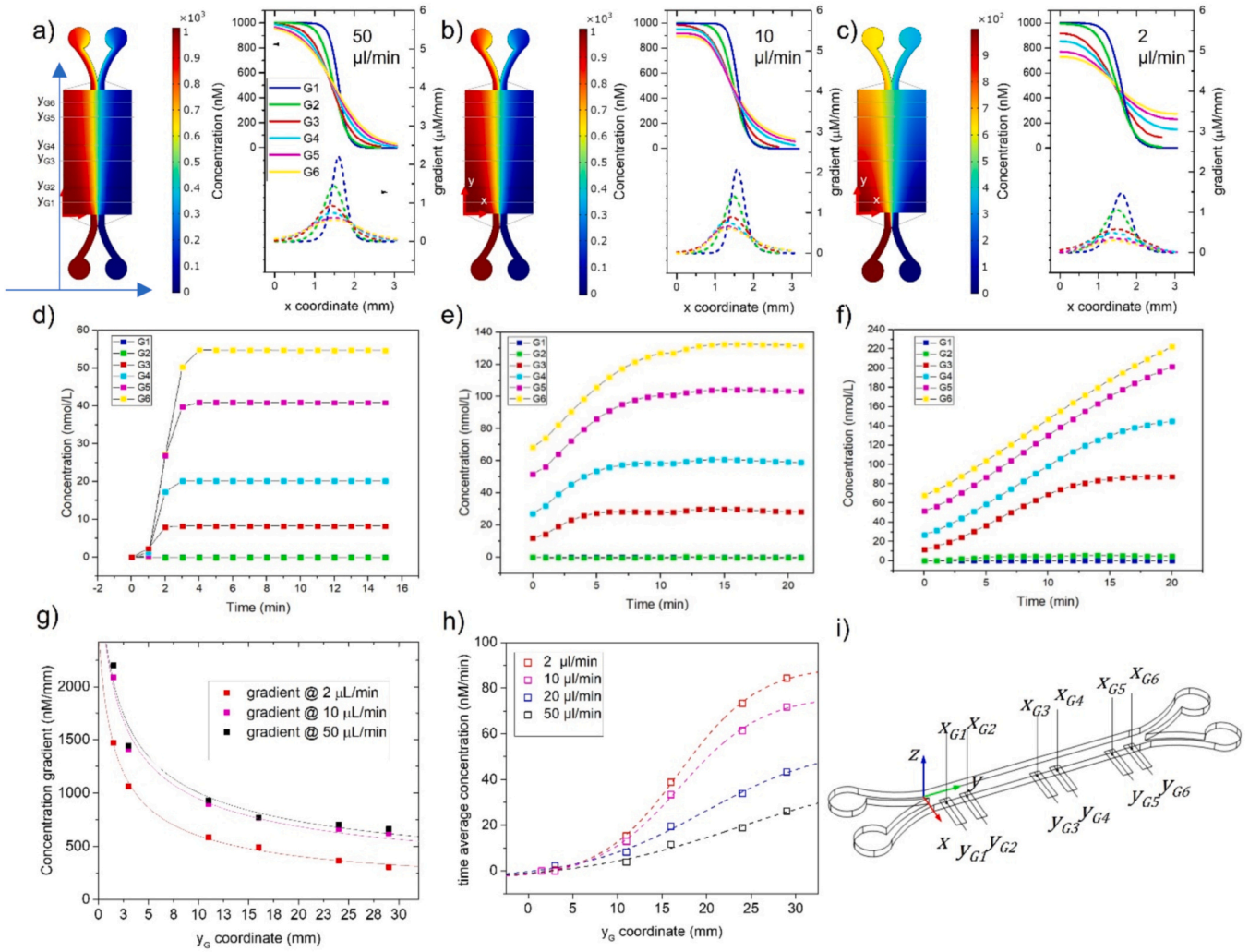

Fig. 2. (a-c) Concentration maps extracted from the COMSOL stationary simulations in the H-cell for flow rate equal to 50 (a), 10 (b), and 2 µl/min (c). The different gate electrodes in the array are marked as G_n, with n = 1 to 6, their symmetry axis being the coordinate y_G. Next to the color maps, the 2D plots show the transversal concentration profile (left axis, continuous lines) and its gradient (right axis, dashed lines) vs x coordinate calculated at different y_G positions. (d-f) Time evolution of concentration at the points (x = 2.5 mm, y_G) from time dependent simulation at different flow rates respectively for 50, 10 and 2 µl/min. g) The value of maximum gradient vs y_G position is plot for each gate of the array. h) Time average concentration vs y_G position calculated with respect to the time of the electrical characterization of each gate electrode. i) Geometry of the H-cell, highlighting the coordinates of the points where the concentration was calculated for the gates immersed inside the microfluidic channel.

Table 1
Main constant parameters adopted for FEM calculation of concentration gradient in H-cell.

Temperature	*Fluid viscosity*	*Initial concentration*	*Diffusion coef.*	*Pressure (outlet)*
***293.15*K**	1mPa·s	1µM	6×10^{-10} m^2/s	10^5 Pa

varying concentration profile across, hence the highest gradient ranging from ≈ 2 µM/mm at G1 to ≈80 nM/mm at G6. The slowest flow rate (Fig. 2c) yields the slowest varying concentration profile across, hence the slowest gradient ranging from ≈ 1.5 µM/mm at G1 to 400 nM/mm. The maximum gradient is at the center of channel ($x = 1.5$ mm), and decreases from G1 to G6.

The adsorption of thiol on the gold gate surface is assumed here to be an irreversible process (viz. the kinetic constant of desorption is disregarded). Hence, the electrode area exposed to the stream acts as a sink for molecules during the duration of the experiment, and the local concentration should be integrated in time to yield the number of molecules deposited on the electrode (indirectly, this yields the coverage of the electrode). During the time of the experiment, the concentration of the solute molecules reaching the microfluidics positions at (x = 2.5, y_G) mm is shown to attain a plateau value in maximum 6 min for high flow rate (50 µl/min) (Fig. 2d) and maximum 12 min for medium flow rate (10 µl/min) (Fig. 2e). It does not reach a plateau and keeps on increasing for the slowest flow rate (2 µl/min) (Fig. 2 f). The dynamic equilibrium determined by adsorption and replenishment by diffusion is controlled by the gradient generated in the microfluidic H-cell. Fig. 2 g shows the gradient at different y_G, with a monotonically decreasing trend. The flow rate affects the gradient only at low flow rates < 10 µl/min. In Fig. 2 h we show the time average concentration profile obtained in the time-dependent simulation. The trend is increasing with respect to y_G coordinate. This allows us to estimate the number of molecules, hence coverage, reaching the substrate just before adsorption.

3.3. EGOFET characterization

Transfer curves were obtained by measuring channel current I_{ds} upon sweeping Gate-Source voltages as reported in Materials and Methods.

The EGOFET transfer curves were acquired in time and correlated with images of diffusion of the thiol solution containing aqueous blue die within the H-cell. The sequence of optical snapshots taken every minute show the gates progressively covered with green color (inset Fig. 3a). In Fig. 3b, the intensity of the green channel calculated across the area of the gate is plotted versus time and correlated with the $I_{ds,max}$ at V_{GS}= −0.7 V. The $I_{ds,max}$ current seems not to be influenced by the diffusing thiol molecules for the initial 3 min, while starts to decrease immediately afterwards, yielding to approximately 82% of the original value, after 8 min. Besides description of what happens when a single gate is subject to a diffusion front, without convective transport, the objective of the present integration was to detect a stable concentration gradient with EGOFET, established by both diffusion and convection. Therefore, all six gates inside H-cell were sequentially used to bias the EGOFET channel. Initially the device was characterised just with PBS for reference. After the thiol solutions were perfused at initial concentration of 1 μM concurrently with PBS, the device characteristics were recorded for the different flow rates in consecutive experiments. Since the device mostly is operated in the linear regime, the response of the EGOFET device is changing with gates exposed to increasing concentration of MP due to thiol concentration gradient build up in the H-cell.

The effect of the flow rate on the thiol adsorption on the gate electrodes can be detected by changes of transistor transfer curves recorded for the respective gate sweeps as shown in Fig. 3c for MP (10 μl/min flux). The I_{ds} recorded when gate 1 was biased does not show a substantial change after injection of thiol solution, with respect to the recording with pristine gate when both inlets are flown with PBS solvent. Since the gradient is steep in the vicinity of gate 1, there is limited diffusion across the interface between the streams, therefore the gate electrode work function remains close to that of clean gold. Only when gate 4 was biased, I_{ds} was significantly reduced by almost 80%. Moreover, the transfer curves recorded with gate 5 and gate 6 show a further decrease in maximum current, valorising the hypothesis that the diffusion induced by the smoother concentration gradient of MP through the interface leads to increased coverage of the organic layer, whose kinetics can be resolved from the analysis of the EGOFET characteristics. The electrical characterization for the other two thiol species MH and MN is also reported in the Supporting Information (Fig. S4 and S5).

It is possible to normalize the output current of the gate exposed to thiol diffusing front with respect to the current of the same gate recorded during the priming of the H-cell with streaming PBS buffer.

The signal S was calculated as the relative current change at V_{GS}= −0.7 V with respect to that measured in pure PBS solvent flow:

$$Signal = \frac{I_{ds,ref} - I_{ds,SAM}}{I_{ds,ref}} \quad (2)$$

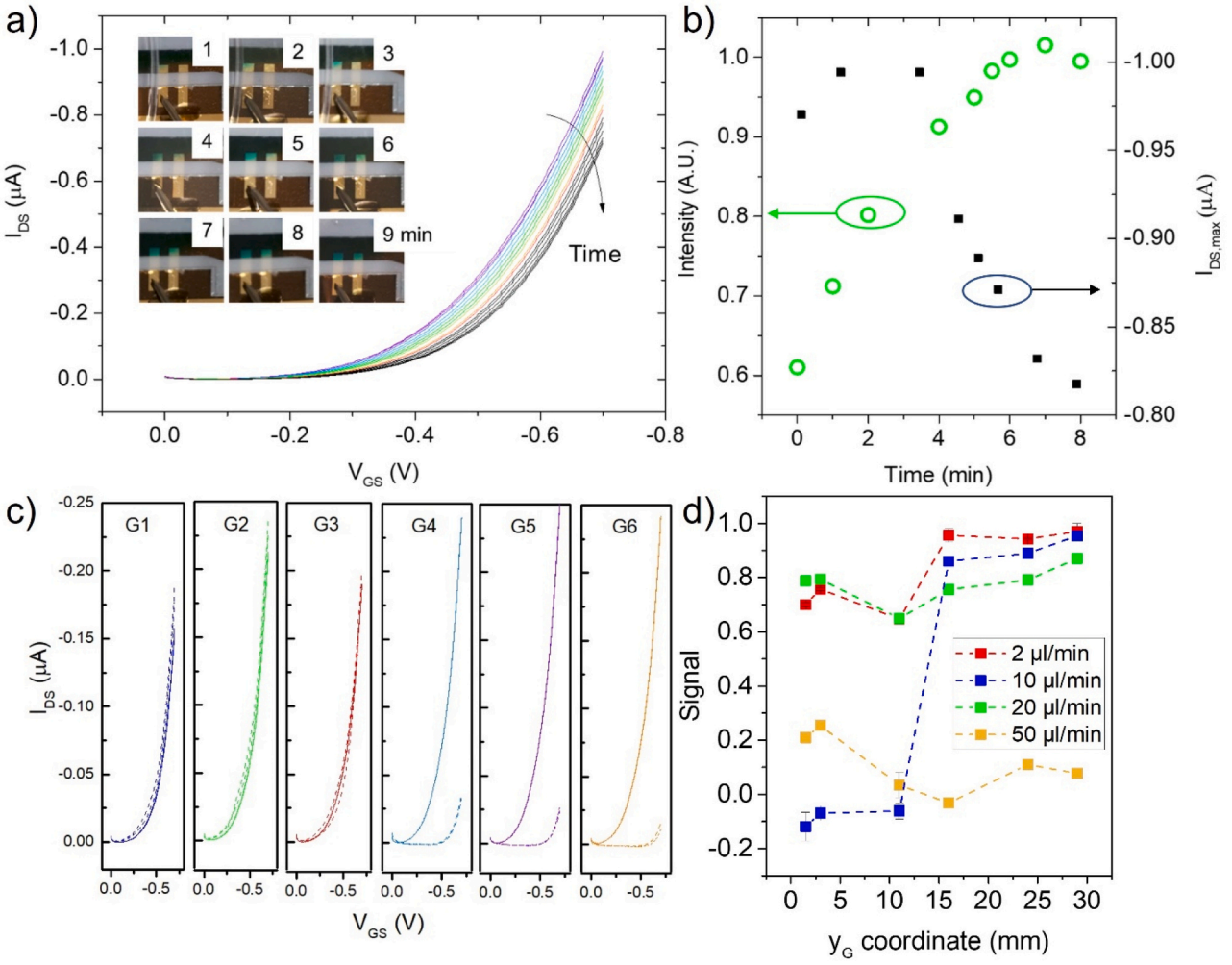

Fig. 3. (a) Transfer curves recorded on gate 5 after taking snapshot of the color die diffusing with thiols along the H-cell channel. In the insets it is possible to recognize a change in color of the solution at different time stamps (b) Correlation between green intensity (left axis) and $I_{ds,max}$ (right axis) for the data reported in a). (c) Transfer curves of EGOFET device for MP at each gate inside the microfluidic channel, flux= 10 μl/min, reported with dashed lines. Solid lines are the reference measurement with PBS buffer; (d) Signal calculations of MP for different flow rates, calculated according to Eq. 4. Dashed lines are provided as guide to the eye.

Where $I_{ds,ref}$ stands for the average of Drain-Source currents recorded for each gate electrode, and $I_{ds,SAM}$ for the corresponding measurement after streaming of thiol solution. The values of S extracted from EGOFET transfer characteristics are reported for each gate position in Fig. 3d. The average signal is calculated for MP after 12 experimental recordings and seems to be grouped at two extremes, either showing values close either to 0 or 1 according to the flow rate and the gate position. For 2 μl/min, S stays in the range between 0.7 and 1 for all the gates measured. For 10 μl/min, S undergoes a shift from low to high signal values after gate 3, and gradually increases up to 0.95. For 20 μl/min, the signal increase is observed after gate 2, but the signal recorded for the first two gates is unexpectedly high, possibly due to an initial unnoticed stream deviation induced by pressure unbalance at the outlets. For 50 μl/min, the average signal is always below 0.3, indicating that the SAM formation is hampered by the insufficient extension of diffusion across the x coordinate, as calculated also from FEM simulation.

For control experiment, a simple microfluidic channel with same length was used. The signal and the shift of threshold voltage of the control experiment with MP are shown in Fig. S6. The plots confirm that without diffusion gradient induced by the H-cell, the SAM formation mediated by thiol adsorption is equal for all the gates. Therefore signal and threshold voltage both remain constant when the concentration gradient is not formed.

Different flow rates induce concentration gradient with specific profile for the different flow rates, as seen in Fig. 2g. The time average concentration has been used as factor for plotting signal vs time in Fig. 4a. With this unconventional scaling, it is possible to clearly distinguish the effect of flow rate on the signal output. The trend for 2 μl/min shows higher normalized signal values, increasing almost linearly within the time of experiment. The signals for 10 and 20 μl/min show a reduced time slope with foreseen plateau level in between 1 and 1.5, whereas for the 2 μl/min, the value of signal times concentration is reaching a value higher than 3. For the flow rate 50 μl/min the normalized signal does not change in time.

In Fig. 4b the signal values are compared between the three different thiol molecules injected at 50 μl/min. Although the MP can be clearly distinguished from MH and MN, considering the absolute value of the signal, the y_G coordinate does not seem to have an effect overall also at the highest flow rate. The analysis at 2 and 20 μl/min for MH and MN did not exhibit similar features as for MP (see Supporting Information), suggesting that the concentration required for observing the signal growth was probably overpassed.

In order to verify the limitation of the kinetics induced by the transport phenomena, and compare the results between the thiol species, EGOFET signal is plotted against the flow rate ϕ for gate 6 (i.e. where the concentration is maximum) (Fig. 4c). A power law decay $S = A\cdot(\alpha - \phi)^{\beta}$ is added to data points to extract a semiquantitative parameter for comparison, which is the exponent β. The rationale is to verify whether the signal is changing considerably with flow rate (transport-limited operative interval) or stays approximately constant with flow rate (reaction-limited operative interval). In Fig. 4c-inset, the exponent extracted from power law fitting is approximately equal to 0.6 for MP, while for MH and MN is approximately 0.4. The signal dependence on flow rate, more appreciable for MP, is suggesting that for this short chain compound there is transport-limited regime, whereas for MH and MN the high signal values and the non-changing signal with respect to flow rate suggest that reaction kinetics were already the limiting factor. Since diffusion constant is similar between the thiol moieties, according to Eq. 31, the different behaviour between MP and the other two compounds might be ascribed to the tendency to form self-assembled monolayer depending on the length of the thiol molecule. Interestingly, in previous studies detailing the effect of viscosity on the electrode transfer rates of protein adsorption on SAMs, a slight difference between the electro transfer rates recorded for MP and MH or MN were similarly reported.

4. Discussion

The mechanism of self-assembly generally occurs in two stages. Initially a fast reaction of adsorption takes place, with various degrees of order depending on the thiol molecule, solvent and concentration [40]. Then, the adsorbed molecules start a reorganization, where they tend to form more compact and ordered assembled domains. The first step is governed by kinetics, the latter by minimization of free energy.

From FEM simulation, we extract a value of thiol concentration of approximately 10 nM near the position of Gate 1 and 2, when operating with flow rate of 2 μl/min. According to a simplistic model of adsorption, for this concentration the time for completion of the self-assembled monolayer is larger than 12 h [31]. Hence, it is reasonable to accept that the amount of MP molecules chemisorbed on the surface in the time of the experiment do not form a layer with high coverage, and its packing

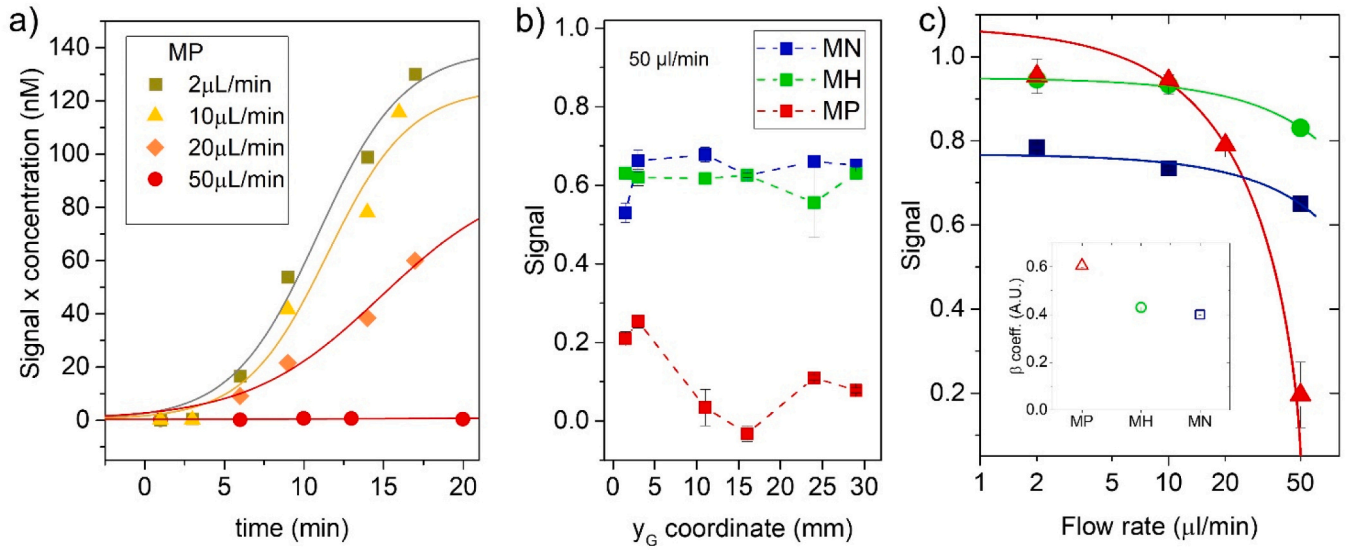

Fig. 4. a) Time evolution of the product between signal and time average concentration, at different flow rates. Continuous lines were best fit with Eq. 7. b) Signal recorded at 50 μl/min is plotted for different thiols MN, MH MP, when device was biased by gates at different y_G coordinate. MP is clearly distinguished form MH and MN c) EGOFET signal versus flow rate plotted for selected gates covered with MP (red triangles), MH (green circles) and MN (blue squares). Continuous lines are the result of fitting the data with the power law model. (inset) The β exponent is reported for the different thiols, error bars are comparable to the symbols.

will be highly disordered. This conclusion is supported by CV results performed in static conditions (inset Fig. S7 in Supporting Information) and also by scanning electrochemical microscopy literature [41]. On the contrary, MH and MN show a signal almost independent on the gate position (Fig. S4 and S5) as they tend to form a more compact SAM. Indeed, the bulk concentration to accomplish high surface coverage for thiol with longer alkyl chain is of the order of 1 nM, which may imply that all electrodes attain a high coverage immediately at the beginning of injection.

To explain the EGOFET signal acquired at different time steps when the gates were exposed to the gradient generated by the H-cell, we adopt an autocatalytic model that was proposed for describing the SAM formation [42]. From Fig. 3b it is possible to appreciate the initial lag where the current is constant, although the rate of colorimetric change determined by diffusion is rapidly changing and reaching a maximum. This confirms that the adsorption process and the reorganization of the electrical double layer is a limiting step with respect to the diffusion process. The autocatalytic model described below, though, does not distinguish between the adsorption from the liquid phase and reorganization of randomly adsorbed molecules.

In the autocatalytic model, the species involved are named as *M*, corresponding to the thiol molecules in the bulk solution and T_{ads}, the thiolated organic layer formed on the gold surface. Alkanethiols adsorption on the gold surface occurs potentially along the boundaries of already formed islands, for this reason we consider as dominant the kinetic contribution related with the self-assembled monolayer formation, with respect to random adsorption. The reaction can be expressed as [43]:

$$M + T_{ads} \underset{g_{des}}{\overset{k_{ads}}{\rightleftharpoons}} 2 \quad T_{ads} \tag{3}$$

With k_{ads} being the kinetic constant for adsorption along the thiol patches borders and g_{des} the desorption constant. The time evolution of species is calculated after integration as:

$$T_{ads}(t) = \frac{b \cdot k \cdot (a+b) e^{((a+b)kt)}}{b \cdot g \cdot e^{((a+b)kt-1)} + b \cdot k \cdot e^{((a+b)kt)} + a \cdot k} \tag{4}$$

Where a and b are representing respectively the values of thiol concentration in solution in proximity of the gate surface and concentration of the adsorbed SAM at $t = 0$. We used a simplified notation for the kinetic constants k and g without subscripts for simplicity of reading. Experimental values for $k_{ads} = 11.5 \times 10^{-3} \quad m^3 \quad (mol\ s)^{-1}$ and $g_{des} = 6 \times 10^{-4} \quad s^{-1}$ were reported in previous works [44]. The concentration of adsorbed thiol shall be slightly different from zero in order for the autocatalytic model to start. In the present kinetic modelling we are not taking into account the effect of viscosity of the medium, since the low gate potential scan is set to avoid electron transfer between the electrolyte solution and the gate electrode, which are only capacitively coupled. Moreover the two fluid streams have the same composition except for 1 μM of thiol in the relevant side.

If we assume coverage $\theta(\zeta, x_G, y_G)$ to be a function of the thiol specie ζ, by which the adsorbed molecules form a self-assembled monolayer on the geometrical surface of the electrode, we have

$$T_{ads}(\tau) = \frac{1}{\tau} \int_0^\tau dt \theta(\zeta, x_G, y_G) \cdot c(x_G, y_G, t) \tag{5}$$

$$T_{ads}(\tau) = \theta(\zeta, x_G, y_G) \cdot \frac{1}{\tau} \int_0^\tau dt c(x_G, y_G, t) \tag{6}$$

where $c(x_G, y_G, t)$ is the concentration in proximity of the gate, in conditions not near the complete depletion of the liquid layer induced by adsorption.

The EGOFET signal S can be directly correlated to the coverage θ attained by the thiol molecules on the gate surface, since the areal extension and structure of the organic layer is affecting the electrical double layer between the gate surface and the electrolyte. In our case, depending on the thiol specie, the larger the coverage is, the larger will be the decrease in I_{ds} and consequently the larger the signal S, as calculated in Eq. 2. Hence, we recast Eq. 6 as

$$T_{ads}(\tau) \approx const \cdot S(x_G, y_G) \cdot \langle c(x_G, y_G, \tau) \rangle \tag{7}$$

Where we assumed a linear response $S(x_G, y_G) \propto \theta(\zeta, x_G, y_G)$ and put the time average concentration $\langle c(x_G, y_G, \tau) \rangle = \frac{1}{\tau} \int_0^\tau dt c(x_G, y_G, t)$ The signal data multiplied by time average concentration were fit with Eq. 4 and the resulting trends are reported in Fig. 4a. In the present analysis, g is held fixed at $6 \times 10^{-4} \quad s^{-1}$. The agreement between the product of experimental/simulation data and the model is good at all flow rates up to 20 μl/min. For 50 μl/min, the curve flattens to zero because the requirements for the autocatalytic model reaction were not fulfilled within the geometry of the H-cell used in the experiment.

In summary, the autocatalytic model, albeit simplistic, explains semi-quantitatively the trend observed of our experimental data, thus supporting the picture where each gate responds to the coverage of the SAM on the gate, and that the H-cell actuates a longitudinal concentration gradient by diffusion.

5. Conclusion

Here, we present EGOFET as an electroanalytical tool for monitoring self-assembly monolayers on top of flexible gold electrodes. The control in time and space of the self-assembled monolayer formation is achieved by means of the diffusion interface within two streams flowing in a laminar flow regime. For this purpose, we integrate the microfluidic H-cell with an array of gate electrodes that are capacitively connected to the organic semiconductor channel of an EGOFET. The H-cell governs the formation of SAMs on the gates by the transversal concentration gradient derived by diffusion from the solute stream to the solvent stream. Since the concentration gradient is varying with flow rate, the effect on the SAM formation is studied by looking at signal from EGOFET. The capability of the GA-EGOFET to detect the diffusion-governed gradient is demonstrated by correlating the results of finite element simulation and the EGOFET signal at the axial positions of the gate electrodes along the microfluidic channel with a simple kinetic model of SAM formation.

Finally the integration of GA-EGOFET with microfluidic device presented in this paper may be regarded as a useful prototype for the systematic automated generation of dose curves, containing as many experimental points as the number of gate electrodes in the array. This approach may indeed be engineered for standardisation of EGOFET or OECT sensors, which is a problem of uttermost importance for the consolidation of these ultrasensitive sensor technology.

CRediT authorship contribution statement

Saygin Gulseren Deniz: Conceptualization, Data curation, Formal analysis, Investigation, Methodology, Writing – original draft, Writing – review & editing. **Greco Pierpaolo:** Conceptualization, Data curation, Formal analysis, Funding acquisition, Investigation, Methodology, Supervision, Validation, Visualization, Writing – original draft, Writing – review & editing. **Selvaraj Meenu:** Data curation, Investigation, Validation, Writing – original draft, Writing – review & editing. **Di Lauro Michele:** Conceptualization, Investigation, Methodology, Writing – original draft. **Murgia Mauro:** Investigation, Resources, Writing – original draft. **Bianchi Michele:** Conceptualization, Investigation, Methodology, Writing – original draft. **Fadiga Luciano:** Conceptualization, Funding acquisition, Methodology, Writing – original draft. **Biscarini Fabio:** Conceptualization, Formal analysis, Funding acquisition, Supervision, Validation, Writing – original draft, Writing – review & editing.

Declaration of Competing Interest

The authors declare that they have no known competing financial interests or personal relationships that could have appeared to influence the work reported in this paper.

Data availability

Data will be made available on request.

Acknowledgments

This work was financially supported by the European Commission through the Marie Sklodowska-Curie ITN projects “BORGES” grant n. 813863 (GDS, PG, MM, MDL, MB, FB) and “AiPBAND” grant n. 7642810 (MS), and by the Neurosciences and Rehabilitation Department of University of Ferrara, through “FIRD2023” (PG).

Appendix A. Supporting information

Supplementary data associated with this article can be found in the online version at doi:10.1016/j.snb.2023.135185.

References

[1] G.M. Whitesides, The origins and the future of microfluidics, Nature 442 (2006) 368–373, https://doi.org/10.1038/nature05058.
[2] A.I. Barbosa, N.M. Reis, micro fluidic immunoassay devices for the sensitive quantitation of protein biomarkers at the point of care, (2017) 858–882. https://doi.org/10.1039/c6an02445a.
[3] S.F. Berlanda, M. Breitfeld, C.L. Dietsche, P.S. Dittrich, Recent Advances in Microfluidic Technology for Bioanalysis and Diagnostics, (2021). https://doi.org/10.1021/acs.analchem.0c04366.
[4] M.A. Tomeh, X. Zhao, Recent Advances in Micro fluidics for the Preparation of Drug and Gene Delivery Systems, (2020). https://doi.org/10.1021/acs.molpharmaceut.0c00913.
[5] A. Bulgakova, A. Berdyugin, O. Naumova, B. Fomin, D. Pyshnyi, A. Chubarov, E. Dmitrienko, A. Lomzov, Solution pH effect on drain-gate characteristics of SOI FET biosensor, Electronics 12 (2023) 777, https://doi.org/10.3390/electronics12030777.
[6] A. Purwidyantri, A. Ipatov, T. Domingues, J. Borme, M. Martins, P. Alpuim, M. Prado, Programmable graphene-based microfluidic sensor for DNA detection, Sens. Actuators B Chem. 367 (2022) 132044, https://doi.org/10.1016/j.snb.2022.132044.
[7] M. Chanda, S.D. Patel, A. Bhattacharyya, S. Sahay, Impact of transport mechanism on binding kinematics and sensitivity of FET biosensors, IEEE Trans. Electron Devices (2023) 1–9, https://doi.org/10.1109/TED.2023.3281539.
[8] Y. Zhou, Q. Lin, Microfluidic flow-free generation of chemical concentration gradients, Sens. Actuators B Chem. 190 (2014) 334–341, https://doi.org/10.1016/j.snb.2013.08.073.
[9] A. Yahyazadeh Shourabi, N. Kashaninejad, M.S. Saidi, An integrated microfluidic concentration gradient generator for mechanical stimulation and drug delivery, J. Sci. Adv. Mater. Devices 6 (2021) 280–290, https://doi.org/10.1016/j.jsamd.2021.02.009.
[10] M.S. Maglione, S. Casalini, S. Georgakopoulos, M. Barbalinardo, V. Parkula, N. Crivillers, C. Rovira, P. Greco, M. Mas-Torrent, Fluid mixing for low-power ‘digital microfluidics’ using electroactive molecular monolayers, Small 14 (2018) 1703344, https://doi.org/10.1002/smll.201703344.
[11] M. Berger, A. Zygmanowski, F. Sellering, H. Röhrich, T. Perl, H. Mansour, S. Zimmermann, Contactless and continuous sodium concentration monitoring during continuous renal replacement therapy, Sens. Actuators B Chem. 320 (2020) 128372, https://doi.org/10.1016/j.snb.2020.128372.
[12] M. Berger, M. Sehlmeyer, F. Sellering, H. Röhrich, T. Perl, H. Mansour, D. Baasner, S. Zimmermann, In-line monitoring of electrolytes and urea during continuous renal replacement therapy, J. Sens. Sens. Syst. 9 (2020) 251–262, https://doi.org/10.5194/jsss-9-251-2020.
[13] V.F. Annese, Integrating Microfluidics and Electronics in Point-of-Care Diagnostics: Current and Future Challenges †, (2022) 1–17.
[14] K.D. Dorfman, D.Z. Adrahtas, M.S. Thomas, C.D. Frisbie, Microfluidic opportunities in printed electrolyte-gated transistor biosensors, Biomicrofluidics 14 (2020), https://doi.org/10.1063/1.5131365.
[15] S. Islam, S. Shukla, V.K. Bajpai, Y. Han, Y.S. Huh, Microfluidic-based graphene field effect transistor for femtomolar detection of chlorpyrifos, Sci. Rep. 7 (1) (2019), https://doi.org/10.1038/s41598-018-36746-w.
[16] J.F.C. Loo, A.H.P. Ho, A.P.F. Turner, W.C. Mak, Integrated printed microfluidic biosensors, Trends Biotechnol. 37 (2019) 1104–1120, https://doi.org/10.1016/j.tibtech.2019.03.009.
[17] V. Parkula, M. Berto, C. Diacci, B. Patrahau, M. Di Lauro, A. Kovtun, A. Liscio, M. Sensi, P. Samor, P. Greco, C.A. Bortolotti, F. Biscarini, Novel Lab-on-Chip Multigate Organic Transistor, (2020). https://doi.org/10.1021/acs.analchem.0c01655.
[18] M. Berto, C. Diacci, R. D’Agata, M. Pinti, E. Bianchini, M.Di Lauro, S. Casalini, A. Cossarizza, M. Berggren, D. Simon, G. Spoto, F. Biscarini, C.A. Bortolotti, EGOFET Peptide aptasensor for label-free detection of inflammatory cytokines in complex fluids, Adv. Biosyst. 2 (2018) 1–8, https://doi.org/10.1002/adbi.201700072.
[19] M. Sensi, M. Berto, S. Gentile, M. Pinti, A. Conti, G. Pellacani, C. Salvarani, A. Cossarizza, C.A. Bortolotti, F. Biscarini, Anti-drug antibody detection with label-free electrolyte-gated organic field-effect transistors, Chem. Commun. 57 (2021) 367–370, https://doi.org/10.1039/d0cc03399e.
[20] E. Macchia, K. Manoli, C. Di Franco, R.A. Picca, O. Ronald, G. Palazzo, F. Torricelli, G. Scamarcio, L. Torsi, Organic Field-E ff ect Transistor Platform for Label-Free, Single- Molecule Detection of Genomic Biomarkers, (2020). https://doi.org/10.1021/acssensors.0c00694.
[21] M. Di Lauro, M. Berto, M. Giordani, S. Benaglia, G. Schweicher, D. Vuillaume, C. A. Bortolotti, Y.H. Geerts, F. Biscarini, Liquid-gated organic electronic devices based on high-performance solution-processed molecular semiconductor, Adv. Electron. Mater. 3 (2017) 1–6, https://doi.org/10.1002/aelm.201700159.
[22] P. Allison, M. Urbina, M. Berto, P. Greco, M. Sensi, S. Borghi, M. Borsari, A. Bortolotti, F. Biscarini, Physical insights from the Frumkin isotherm applied to electrolyte gated organic transistors as protein biosensors †, (2021) 10965–10974. https://doi.org/10.1039/d1tc02546e.
[23] K. Solodka, M. Berto, D. Ferraro, C. Menozzi, M. Borsari, C.A. Bortolotti, F. Biscarini, M. Pinti, Detection of Neurofilament Light Chain with Label-Free Electrolyte-Gated Organic Field-Effect Transistors, (2022). https://doi.org/10.1002/admi.202102341.
[24] M. Berto, E. Vecchi, L. Baiamonte, C. Condò, M. Sensi, M. Di Lauro, M. Sola, A. De Stradis, F. Biscarini, A. Minafra, C.A. Bortolotti, Label free detection of plant viruses with organic transistor biosensors, Sens. Actuators B Chem. 281 (2019) 150–156, https://doi.org/10.1016/j.snb.2018.10.080.
[25] S. Casalini, A.C. Dumitru, F. Leonardi, C.A. Bortolotti, E.T. Herruzo, A. Campana, R.F. De Oliveira, T. Cramer, R. Garcia, F. Biscarini, Multiscale sensing of antibody-antigen interactions by organic transistors and single-molecule force spectroscopy, ACS Nano 9 (2015) 5051–5062, https://doi.org/10.1021/acsnano.5b00136.
[26] S. Ricci, S. Casalini, V. Parkula, M. Selvaraj, G.D. Saygin, P. Greco, F. Biscarini, M. Mas-Torrent, Label-free immunodetection of α-synuclein by using a microfluidics coplanar electrolyte-gated organic field-effect transistor, Biosens. Bioelectron. 167 (2020) 112433, https://doi.org/10.1016/j.bios.2020.112433.
[27] M. Selvaraj, P. Greco, M. Sensi, G.D. Saygin, N. Bellassai, R. D’Agata, G. Spoto, F. Biscarini, Label free detection of miRNA-21 with electrolyte gated organic field effect transistors (EGOFETs), Biosens. Bioelectron. 182 (2021) 113144, https://doi.org/10.1016/j.bios.2021.113144.
[28] S. Casalini, C.A. Bortolotti, F. Leonardi, F. Biscarini, Self-assembled monolayers in organic electronics, Chem. Soc. Rev. 46 (2017) 40–71, https://doi.org/10.1039/c6cs00509h.
[29] F. Leonardi, A. Tamayo, S. Casalini, M. Mas-Torrent, Modification of the gate electrode by self-assembled monolayers in flexible electrolyte-gated organic field effect transistors: work function: Vs. capacitance effects, RSC Adv. 8 (2018) 27509–27515, https://doi.org/10.1039/c8ra05300f.
[30] C. Liu, Y. Xu, Y. Noh, Contact engineering in organic field-effect transistors, Mater. Today 18 (2015) 79–96, https://doi.org/10.1016/j.mattod.2014.08.037.
[31] S. Asiaei, P.M. Nieva, Studying the kinetics of thiols’ self-assembled monolayer formation in microfluidic channels, Part. Sci. Technol. 34 (2016) 397–406, https://doi.org/10.1080/02726351.2015.1089964.
[32] T. Frommelt, M. Kostur, M. Wenzel-Schäfer, P. Talkner, P. Hänggi, A. Wixforth, Microfluidic mixing via acoustically driven chaotic advection, Phys. Rev. Lett. 100 (2008) 1–4, https://doi.org/10.1103/PhysRevLett.100.034502.
[33] K. Ward, Z.H. Fan, Mixing in microfluidic devices and enhancement methods, J. Micromech. Microeng. 25 (2015), https://doi.org/10.1088/0960-1317/25/9/094001.
[34] A. Roda, P. Greco, P. Simoni, V. Marassi, G. Moroni, A. Gioiello, B. Roda, Compact miniaturized bioluminescence sensor based on continuous air-segmented flow for real-time monitoring: application to bile salt hydrolase (BSH) activity and ATP detection in biological fluids, Chemosensors 9 (2021) 122, https://doi.org/10.3390/chemosensors9060122.
[35] L.L. Fan, X.L. Zhu, H. Zhao, J. Zhe, L. Zhao, Rapid microfluidic mixer utilizing sharp corner structures, Microfluid. Nanofluidics. 21 (2017) 1–12, https://doi.org/10.1007/s10404-017-1874-y.
[36] B. Farshchian, A. Amirsadeghi, J. Choi, D.S. Park, N. Kim, S. Park, 3D nanomolding and fluid mixing in micromixers with micro-patterned microchannel walls, Nano Converg. 4 (2017) 0–9, https://doi.org/10.1186/s40580-017-0098-x.
[37] J. Marschewski, S. Jung, P. Ruch, N. Prasad, S. Mazzotti, B. Michel, D. Poulikakos, Mixing with herringbone-inspired microstructures: overcoming the diffusion limit in co-laminar microfluidic devices, Lab. Chip. 15 (2015) 1923–1933, https://doi.org/10.1039/c5lc00045a.
[38] C. Cerjan, R.E. Barnett, Viscosity dependence of a putative diffusion-limited reaction, J. Phys. Chem. 76 (1972) 1192–1195, https://doi.org/10.1021/j100652a018.
[39] A. Avila, B.W. Gregory, K. Niki, T.M. Cotton, An electrochemical approach to investigate gated electron transfer using a physiological model system: cytochrome c immobilized on carboxylic acid-terminated alkanethiol self-assembled monolayers on gold electrodes, J. Phys. Chem. B. 104 (2000) 2759–2766, https://doi.org/10.1021/jp992591p.

[40] C.-A. Palma, J. Bjork, M. Bonini, M.S. Dyer, A. Llanes-Pallas, D. Bonifazi, M. Persson, P. Samorì, Tailoring bicomponent supramolecular nanoporous networks: phase segregation, polymorphism, and glasses at the solid−liquid interface, J. Am. Chem. Soc. 131 (2009) 13062–13071, https://doi.org/10.1021/ja9032428.
[41] H. Kumakli, A. Hoque, R.J. White, Observing real-time formation of self-assembled monolayers on polycrystalline gold surfaces with scanning electrochemical cell microscopy, Langmuir 38 (2022) 9148–9156, https://doi.org/10.1021/acs.langmuir.2c00667.
[42] J.F. Douglas, K. Efimenko, D.A. Fischer, F.R. Phelan, J. Genzer, Propagating waves of self-assembly in organosilane monolayers, Proc. Natl. Acad. Sci. 104 (2007) 10324–10329, https://doi.org/10.1073/pnas.0703620104.
[43] J.I. Steinfeld, J.S. Francisco, W.L. Hase, Chemical Kinetics and Dynamics, Prentice Hall, 1999.
[44] F.S. Damos, R.C.S. Luz, L.T. Kubota, Determination of thickness, dielectric constant of thiol films, and kinetics of adsorption using surface plasmon resonance, Langmuir 21 (2005) 602–609, https://doi.org/10.1021/la0487038.

Gulseren Deniz Saygin, Early Stage Researcher in Marie Skłodowska-Curie Action, Phd in Physics and Nanosciences at University of Modena and Reggio Emilia. Her research focuses on the integration of microfluidic devices and biosensors based on organic electronics

Pierpaolo Greco, Researcher at University of Ferrara, associate with Italian Institute of Technology. His research focuses on organic electronic devices, microfabrication with laser technology and biosensor development.

Meenu Selvaraj, Early Stage Researcher in Marie Skłodowska-Curie Action, Phd in Chemical Sciences at University of Catania. Her research focuses on organic electronics devices, microfluidic devices fabrication and integration with optical biosensors

Michele Di Lauro, Researcher at the Italian Institute of Technology. His research focuses on brain machine interfaces development, organic electronic devices for neuromorphic applications, biosensor development and physical chemistry.

Mauro Murgia, Research Engineer at the Italian Institute of Technology. His research focuses on microfabrication with laser technology, high vacuum sublimation of organic and inorganic materials, machine development.

Michele Bianchi, assistant professor of Inorganic Chemistry at University of Modena and Reggio Emilia. His research activity includes the design of microstructured and nanostructured biomaterials for cell guidance, biointerfaces and devices by additive and unconventional fabrication methods.

Luciano Fadiga, Full Professor of Human Physiology at the University of Ferrara, Center Coordinator of the Italian Institute of Technology in Ferrara. His long research experience is in electrophysiology and neurophysiology in monkeys and humans (transcranial magnetic stimulation, study of spinal excitability, brain imaging, recording of single neurons in awake neurosurgery patients).

Fabio Biscarini, Senior Researcher-Principal Investigator (PI) at Italian Institute of Technology in Ferrara, and Full Professor of General and Inorganic Chemistry at University of Modena and Reggio Emilia. His research interests span across physical chemistry and nanotechnology: theories of liquid crystals and STM, to experimental activity in fundamentals of thin film growth, self-organization, and organic electronics devices.